ARTICLE OPEN

Check for updates

Linking altered neuronal and synaptic properties to nicotinic receptor Alpha5 subunit gene dysfunction: a translational investigation in rat mPFC and human cortical layer 6

Danqing Yang[1,2,6]✉, Guanxiao Qi[1,6], Daniel Delev[3], Uwe Maskos[4] and Dirk Feldmeyer[1,2,5]✉

Genetic variation in the α5 nicotinic acetylcholine receptor (nAChR) subunit of mice results in behavioral deficits linked to the prefrontal cortex (PFC). rs16969968 is the primary Single Nucleotide Polymorphism (SNP) in *CHRNA5* strongly associated with nicotine dependence and schizophrenia in humans. We performed single cell-electrophysiology combined with morphological reconstructions on layer 6 (L6) excitatory neurons in the medial PFC (mPFC) of wild type (WT) rats, rats carrying the human coding polymorphism rs16969968 in *Chrna5* and α5 knockout (KO) rats. Neuronal and synaptic properties were determined for the three rat genotypes. Compared with neurons in WT rats, L6 regular spiking (RS) neurons in the α5KO group exhibited altered electrophysiological properties, while those in α5SNP rats remained unchanged. L6 RS neurons in mPFC of α5SNP and α5KO rats differed from WT rats in dendritic morphology, spine density and spontaneous synaptic activity. Galantamine was applied to identified L6 neuron populations to specifically boost the nicotinic responses mediated by α5*nAChRs. Remarkably, it restored nicotinic modulation in neurons of α5SNP rats, while no such effect was observed in α5KO rats. Additionally, galantamine functioned as a positive allosteric modulator of α5*nAChRs in RS neurons, both in rat and human cortical L6, but did not affect burst spiking (BS) neurons. Our findings suggest that dysfunction in the α5 subunit gene leads to aberrant neuronal and synaptic properties, shedding light on the underlying mechanisms of cognitive deficits observed in human populations carrying α5SNPs. They highlight a potential pharmacological target for restoring the relevant behavioral output.

Translational Psychiatry (2025)15:12 ; https://doi.org/10.1038/s41398-025-03230-9

INTRODUCTION

Acetylcholine (ACh) is believed to play a critical role in memory processing, arousal, attention, learning, and sensory signaling through activating both muscarinic and nicotinic ACh receptors (AChRs) [1–5]. The medial prefrontal cortex (mPFC) is one of the various brain cortices affected by cholinergic modulation, and it is essential for working memory and top-down attention [6, 7]. The mPFC is densely innervated by cholinergic axons originating from the basal forebrain, and ACh release in this brain area has been linked to cue detection and attentional performance [8–10]. nAChRs are transmembrane ionotropic receptors activated by ACh and nicotine. The most widely expressed nAChRs in the brain are the hetero-pentameric α4β2* nAChRs [11–13]. In the relatively rare brain regions including deep layers of mPFC, some of α4β2* nAChRs contains the α5 subunit encoded by the *Chrna5* gene [14, 15]. The co-assembly of α5 subunits enhances the Ca^{2+} permeability of the receptor, increases the receptor affinity for ACh, and slows down the receptor desensitization [16–18].

Several neuropsychiatric disorders have been linked to coding and non-coding Single Nucleotide Polymorphisms (SNPs) in human CHRNA5 in a number of comprehensive Genome-wide Association Studies (GWAS) (for a review see [19]). In addition to a robust association with smoking-related diseases [20–23], these SNPs are strongly implicated in mental disorders with cognitive deficits such as schizophrenia (SZ) [24–28]. Among these variants, the rs16969968 SNP leads to the substitution of aspartic acid by asparagine at residue 398 (D398N) in the human α5 subunit, resulting in partial loss of function of α5-containing nAChRs [29]. This SNP is highly prevalent in humans, especially in populations of European descent with an approximately frequency of 35% [29]. rs16969968 is the primary SNP in *CHRNA5* that is strongly associated with nicotine dependence and smoking-related behaviors [29–31]. It also shows modest associations with schizophrenia. Other SNPs in *CHRNA5*, such as rs684513, rs17487223, and rs951266, show weaker and less consistent associations with these conditions [32–34]. In humans and animal models with this SNP, reduced resting-state functional connectivity and alterations in circuits involving the PFC were found [35, 36]. These rodents self-administered higher doses of nicotine and showed cognitive behavioral deficits in tasks related to social interaction and sensorimotor gating [36, 37]. Hence, it is essential

[1]Research Center Juelich, Institute of Neuroscience and Medicine 10, Research Center Juelich, Juelich, Germany. [2]Department of Psychiatry, Psychotherapy, and Psychosomatics, RWTH Aachen University Hospital, Aachen, Germany. [3]Department of Neurosurgery, Faculty of Medicine, RWTH Aachen University Hospital, Aachen, Germany. [4]Institut Pasteur, Université de Paris Cité, Neurobiologie Intégrative des Systèmes Cholinergiques, CNRS UMR3571, Paris, Cedex 15, France. [5]Jülich-Aachen Research Alliance, Translational Brain Medicine (JARA Brain), Aachen, Germany. [6]These authors contributed equally: Danqing Yang, Guanxiao Qi. ✉email: d.yang@fz-juelich.de; d.feldmeyer@fz-juelich.de

Received: 6 May 2024 Revised: 9 December 2024 Accepted: 10 January 2025
Published online: 17 January 2025

to investigate how rs16969968 SNP alters the cellular and synaptic mechanisms in the PFC that underlie behavioral deficits.

A robust feedback projection to the thalamus originates in layer 6 (L6) of the prefrontal cortex and is often disrupted in SZ [38, 39]. L6 of the PFC is one of the few brain regions expressing α5* nAChRs, with certain neurons specifically expressing α4β2α5 nAChRs [14, 15]. In mice, deletion of the α5 nAChR subunit gene *Chrna5* results in reduced cholinergic excitation and aberrant neuronal morphology in L6 of the PFC [18, 36, 40, 41]. However, it remains unclear whether rs16969968 SNP can induce neuronal pathophysiology and altered nicotinic signaling in this neuron population. In this study, we performed whole-cell recordings on L6 excitatory neurons in the rat mPFC using a transgenic rat line expressing rs16969968 α5SNP [37] and compared it with wild-type and *Chrna5* knock-out rats. This approach allowed us to study the effect of this variant on neuronal electrophysiology, morphology, and nicotinic signaling. The positive allosteric modulator (PAM) galantamine, which specifically targets nAChRs containing the α5 subunit, was used in rat and human cortical L6 to investigate the neuronal dysfunctions underlying the cognitive deficits observed in human α5SNPs, with the aim of identifying pharmacological effectors that could potentially restore behavioral performance.

MATERIALS AND METHODS

Animals and patients

All experimental procedures involving animals were performed in accordance with the guidelines of the Federation of European Laboratory Animal Science Association, the EU Directive 2010/63/EU, and the German animal welfare law. Wild type (WT) Long-Evans rats were purchased from Janvier Lab. α5KO and α5SNP Long-Evans rats were generated and housed at Institut Pasteur, Paris, France [37] and homozygous rats were bred at Research Centre Juelich, Juelich, Germany. Male and female Long-Evans WT, α5KO, and α5SNP rats aged 28–105 postnatal days were used for experiments. All rats were individually housed in a temperature-controlled environment on a 12-h reverse light-dark cycle, with food and water available ad libitum. No specific blinding was performed during the animal experiments.

All patients underwent neurosurgical resections because of hippocampus sclerosis or tumor removal. Written informed consent to use spare neocortical tissue acquired during the surgical approach was obtained from all patients. The study was reviewed and approved by the ethic committee of RWTH Aachen University Hospital (EK067/20). The cases were meticulously selected to fulfill two main criteria: 1) availability of spare tissue based on the needed surgical approach; and 2) normal appearance of the tissue according to radiological and intraoperative criteria (absence of edema, absence of necrosis, and distance to any putative intracerebral lesion). In addition, samples from tumor cases were neuropathologically reviewed to rule out the presence of tumor cells in the examined neocortical specimen. Within the constraints of surgical necessity and tissue availability, we randomly selected eligible patients to minimize selection bias. Where possible, tissue samples were assessed blindly by neuropathologists to prevent any preconceived notions or biases from influencing the evaluation of tissue normality. The selection criteria were strictly adhered to all cases to avoid subjective bias. The criteria focused on obtaining tissue that appeared normal both radiologically and intraoperatively, ensuring uniformity across samples. Patients of different ages, genders, and medical backgrounds were included to ensure the samples were representative of the broader population undergoing such neurosurgical procedures. By implementing these measures, we aimed to minimize potential biases in our sample selection.

Slice preparation

Rats were deeply anaesthetized with isoflurane, decapitated, and the brain was rapidly removed. Human cortical tissue was micro-dissected and resected with minimal use of bipolar forceps to ensure tissue integrity. Rat and human neocortical tissue blocks were directly transferred into an ice-cold artificial cerebrospinal fluid (ACSF), which was either sucrose- or choline-based, respectively. The choline-based ACSF contained (in mM): 110 choline chloride, 26 $NaHCO_3$, 10 D-glucose, 11.6 Na-ascorbate, 7 $MgCl_2$, 3.1 Na-pyruvate, 2.5 KCl, 1.25 NaH_2PO_4, and 0.5 $CaCl_2$) (325 mOsm/l, pH 7.45).

To dissect human brain tissue, the pia was removed using forceps, and the pia-white matter (WM) axis was identified. 300 µm or 350 µm thick slices were prepared using a Leica VT1200 vibratome in ice-cold sucrose-based ACSF solution containing (in mM): 206 sucrose, 2.5 KCl, 1.25 NaH_2PO_4, 3 $MgCl_2$, 1 $CaCl_2$, 25 $NaHCO_3$, 12 N-acetyl-L-cysteine, and 25 glucose (325 mOsm/l, pH 7.45). During slicing, the solution was constantly bubbled with carbogen gas (95% O_2 and 5% CO_2). After cutting, slices were incubated for 30 min at 31–33 °C and then at room temperature in ACSF containing (in mM): 125 NaCl, 2.5 KCl, 1.25 NaH_2PO_4, 1 $MgCl_2$, 2 $CaCl_2$, 25 $NaHCO_3$, 25 D-glucose, 3 myo-inositol, 2 sodium pyruvate, and 0.4 ascorbic acid (300 mOsm/l; 95% O_2 and 5% CO_2). To maintain adequate oxygenation and a physiological pH level, slices were kept in carbogenated ACSF (95% O_2 and 5% CO_2) during transportation.

Whole-cell recordings

Whole cell recordings were performed in acute slices of rat and human neocortex. The recordings were conducted within 8 h after slice preparation for rat neocortex and 30 h at most for human neocortical tissue. During whole-cell patch-clamp recordings, rat or human slices were continuously perfused (perfusion speed ~5 ml/min) with ACSF bubbled with carbogen gas and maintained at 30–33 °C. Patch pipettes were pulled from thick wall borosilicate glass capillaries and filled with an internal solution containing (in mM): 135 K-gluconate, 4 KCl, 10 HEPES, 10 phosphocreatine, 4 Mg-ATP, and 0.3 GTP (pH 7.4 with KOH, 290–300 mOsm). Neurons were visualized using either Dodt gradient contrast or infrared differential interference contrast microscopy. In rat acute prefrontal cortical slices, cortical layers were distinguished by cell density and soma size, in accordance with previous studies on the PFC [42–45]. The PFC can be divided into three sections: the upper third comprises L1–L3, the middle third L5, and the lower third L6. Human L6 neurons were identified and patched according to their somatic location [46]. Putative excitatory neurons and interneurons were differentiated based on their intrinsic action potential (AP) firing pattern during recording and their morphological appearance after post hoc histological staining. Interneurons were excluded from the analysis.

Whole-cell patch clamp recordings of human or rat L6 neurons were made using an EPC10 amplifier (HEKA). During recording, slices were perfused in ACSF at 31–33 °C. Signals were sampled at 10 kHz, filtered at 2.9 kHz using Patchmaster software (HEKA), and later analyzed offline using Igor Pro software (Wavemetrics). Recordings were performed using patch pipettes of resistance between 5 and 10 MΩ. Biocytin was added to the internal solution at a concentration of 3–5 mg/ml to stain patched neurons. A recording time > 15 min was necessary for an adequate diffusion of biocytin into dendrites and axons of patched cells [47].

Drug application

Acetylcholine was bath applied (10 µM) for 150–300 s through the perfusion system or puff applied (100 µM or 1 mM) during whole-cell patch clamp recordings. To specifically investigate the nicotinic effect of ACh, 200 nM atropine was bath applied to block the muscarinic responses. Tetrodotoxin (TTX, 0.5 µM) was added into perfusion ACSF for puff-application experiments to block AP firing induced by high concentrations of ACh. The puff pipette was placed at 10–20 µm from the recorded neuron, and a pressure of 0.5 bar was applied for about 1 s. When different concentrations of ACh were administered to the same neuron, a second puff pipette from the same pulling pair was replaced to ensure uniformity in the electrode's opening size. Galantamine (1 µM) was used as a PAM of α_5*nAChRs. Drugs were purchased from Sigma-Aldrich or Tocris.

Histological staining

After recordings, brain slices containing biocytin-filled neurons were fixed for at least 24 h at 4 °C in 100 mM phosphate buffer solution (PBS, pH 7.4) containing 4% paraformaldehyde (PFA). After rinsing several times in 100 mM PBS, slices were treated with 1% H_2O_2 in PBS for about 20 min to reduce any endogenous peroxidase activity. Subsequently, slices were rinsed repeatedly with PBS and then incubated in 1% avidin-biotinylated horseradish peroxidase (Vector ABC staining kit, Vector Lab. Inc.) containing 0.1% Triton X-100 for 1 h at room temperature. The reaction was catalyzed using 0.5 mg/ml 3,3-diaminobenzidine (DAB; Sigma-Aldrich) as a chromogen. Subsequently, slices were rinsed with 100 mM PBS, followed by slow dehydration with ethanol in increasing concentrations, and finally

in xylene for 2–4 h [47]. After that, slices were embedded using Eukitt medium (Otto Kindler GmbH).

Morphological 3D reconstructions and spine counting

Using NEUROLUCIDA® software (MBF Bioscience, Williston, VT, USA), morphological three-dimensional reconstructions of biocytin filled rat and human L6 excitatory neurons were made at a magnification of 1000-fold (100-fold oil-immersion objective and 10-fold eyepiece) on an upright microscope. Neurons were selected for reconstruction based on the quality of biocytin labeling when background staining was minimal. Neurons with major dendritic truncations due to slicing were excluded. Embedding with Eukitt medium reduced fading of cytoarchitectonic features and enhanced contrast between layers [47]. This allowed the reconstruction of different layer borders along with the neuronal reconstructions. Furthermore, the position of soma and layers was confirmed by superimposing the Dodt gradient contrast or differential interference contrast images taken during the recording. The tissue shrinkage was corrected using correction factors of 1.1 in the x–y direction and 2.1 in the z direction [47]. The spine counting was done using NEUROLUCIDA® software (MBF Bioscience, Williston, VT, USA). All dendritic spines were counted for at least 100 µm along a branch of both apical dendritic tuft and basal dendrite for each neuron. The spine density analysis was performed by using NEUROEXPLORER® software (MBF Bioscience, Williston, VT, USA).

Data analysis

Whole-cell recording data analysis. Custom written macros for Igor Pro 6 (WaveMetrics) were used to analyze the recorded electrophysiological signals. The resting membrane potential (V_m) of the neuron was measured directly after breakthrough to establish the whole-cell configuration with no current injection. The input resistance was calculated as the slope of the linear fit to the current–voltage relationship. For the analysis of single spike characteristics such as threshold, amplitude, and half-width, a step size increment of 10 pA for current injection was applied to ensure that the AP was elicited very close to its rheobase current. The spike threshold was defined as the point of start of acceleration of the membrane potential using the second derivative (d^2V/dt^2), that is, using 3x standard deviation of d^2V/dt^2 as cut-off point. The spike amplitude was calculated as the difference in voltage from AP threshold to the peak during depolarization. The spike half-width was determined as the time difference between rising phase and decaying phase of the spike at half-maximum amplitude.

The spontaneous activity was analyzed using the program SpAcAn (https://www.wavemetrics.com/project/SpAcAn). A threshold of 0.2 mV was set manually for detecting EPSP events.

Dendritic morphology and spine analysis. The horizontal dendritic fieldspan was defined as the widest distance between apical or basal dendrites, measured parallel to the pia. The vertical dendritic fieldspan was defined as the longest distance between apical tuft and basal dendrite, measured perpendicular to the pia. The aspect ratio of the dendritic fieldspan was calculated by dividing the vertical fieldspan by the horizontal fieldspan. Other morphological parameters such as total dendritic length, number of basal dendrites, soma area, and spine density were analyzed with NEUROEXPLORER® software (MBF Bioscience, Williston, VT, USA).

Statistical analysis. Data was either presented as box plots ($n \geq 10$) or as bar histograms ($n < 10$). For box plots, the interquartile range (IQR) is shown as box, the range of values within 1.5∗IQR is indicated by whiskers and the median is represented by a horizontal line in the box; for bar histograms, the mean ± SD is given. Wilcoxon Mann-Whitney U test was performed to assess the difference between individual groups. To assess the differences between two paired groups under different pharmacological conditions, Wilcoxon signed-rank test was performed. Statistical significance was set at $^*P < 0.05$, with $^{**}P < 0.01$ and $^{***}P < 0.001$ indicating higher levels of significance. Results were considered non-significant when $P > 0.05$ (denoted as 'ns' or 'not significant'). n indicates the number of neurons analyzed. Power calculations were conducted to determine the necessary sample sizes for the Wilcoxon test. The effect size was estimated based on means and standard deviations, assuming normal distributions. The required sample size was determined with an α level of 0.05 and a desired power of 0.8. The calculations for sample size and power were performed following the previously published guidelines [48].

RESULTS

Comparing electrophysiology and morphology of mPFC L6 RS neurons in WT, α5SNP and α5KO rats

To investigate whether the expression of the α5 nAChR subunit affects the electrophysiological characteristics of L6 neurons in medial prefrontal cortex (mPFC), we prepared acute brain slices from rats that were either wild-type (WT), carrying the human coding polymorphism rs16969968 in *Chrna5* (α5SNP), or constitutively lacking the α5 subunit (α5KO) [37] (Fig. 1A). L6 excitatory neurons comprise various electro-morphological subtypes and neurons showing different firing patterns also exhibit distinct passive properties [49–52]. Here we focused on analyzing the intrinsic properties of the L6 regular spiking (RS) excitatory neurons (Fig. 1C), which are considered to be corticothalamic (CT) projecting neurons and are known to express the α5 nAChR subunit encoded by *Chrna5* [15, 53, 54]. L6 RS neurons in α5KO rats exhibited the most depolarized resting membrane potential (Vrest, −65.0 ± 7.0 mV) among the three rat genotypes (−71.7 ± 4.2 mV for WT and −69.7 ± 4.0 mV for α5SNP). Correspondingly, L6 RS neurons in α5KO rats demonstrated significantly increased excitability, as evidenced by smaller rheobase currents compared to the WT (58.4 ± 29.3 vs. 87.7 ± 24.9 pA, $^{**}P < 0.01$) and α5SNP group (58.4 ± 29.3 pA vs. 86.0 ± 29.1 pA, $^*P < 0.05$), respectively (Fig. 1B, F). The input resistance (R_{in}) of L6 RS neurons in the α5KO group was significantly higher than R_{in} of neurons in WT (330 ± 60 vs. 251 ± 44, $^{***}P < 0.001$) or α5SNP (330 ± 60 vs. 255 ± 70, $^{**}P < 0.01$) rats (Fig. 1D, F). During hyperpolarizing current injection, the L6 RS neuron in the α5KO rat shows a larger hyperpolarizing voltage sag, and a larger depolarizing overshoot, compared to neurons in the other two genotypes. Specifically, L6 RS neurons in the α5KO group exhibited the most pronounced voltage sag (V_{sag}, 1.65 ± 1.82 mV), which was more than twice that of neurons in the WT (0.70 ± 0.69 mV) or α5SNP (0.65 ± 0.34 mV) group (Fig. 1E, F), suggesting an enhanced or altered regulation of the hyperpolarization-activated inward current (I_h). The overshoot further supports the involvement of I_h in membrane potential recovery, indicating that differences in Ih activation may underlie the sag variations between genotypes.

Furthermore, neurons in the α5KO group exhibited a significantly smaller action potential (AP) amplitude compared to those in the WT group (89.8 ± 6.4 vs. 94.5 ± 5.2 mV, $^*P < 0.05$). Additionally, they displayed a significantly longer onset time (339 ± 129 vs. 219 ± 173 ms, $^*P < 0.05$) for the first AP evoked by injecting a rheobase current. In contrast to the increased excitability observed in L6 RS neurons of the α5KO group, no significant differences were observed in the electrophysiological properties between neurons in the WT and α5SNP groups (Table S1). This suggests that the deletion of *Chrna5* has an impact on the electrophysiological characteristics of L6 RS neurons in the rat mPFC, while those in rats expressing the human SNP remain unaffected.

It has been shown that the α5 subunit plays an important role in normal developmental changes of the dendritic morphology of L6 pyramidal cells. These differences in dendritic morphology can be observed from early adulthood between WT and α5KO mice [55]. To study the impact of the rs16969968 polymorphism on neuronal morphology, we reconstructed the 3D somatodendritic morphology of L6 RS neurons in the mPFC of young adult WT, α5SNP, and α5KO rats. As shown in Fig. 2A, apical dendrites of L6 RS neurons in WT group often terminate before reaching cortical layer 1 (L1, 55%). In contrast, all α5SNP and 80% α5KO rats exhibit long apical dendrites extending into L1 of the mPFC (Fig. 2A, B). There is a gradual decrease of the horizontal dendritic fieldspan that correlates with the reduced presence of functional α5*nAChRs and therefore a gradual increase in the aspect ratio of the dendritic fieldspan across the WT, α5SNP to α5KO groups (Fig. 2A, C). Neurons in both α5SNP and α5KO groups showed a larger number of basal dendrites compared to those in WT rats. However, due to a markedly narrower horizontal dendritic

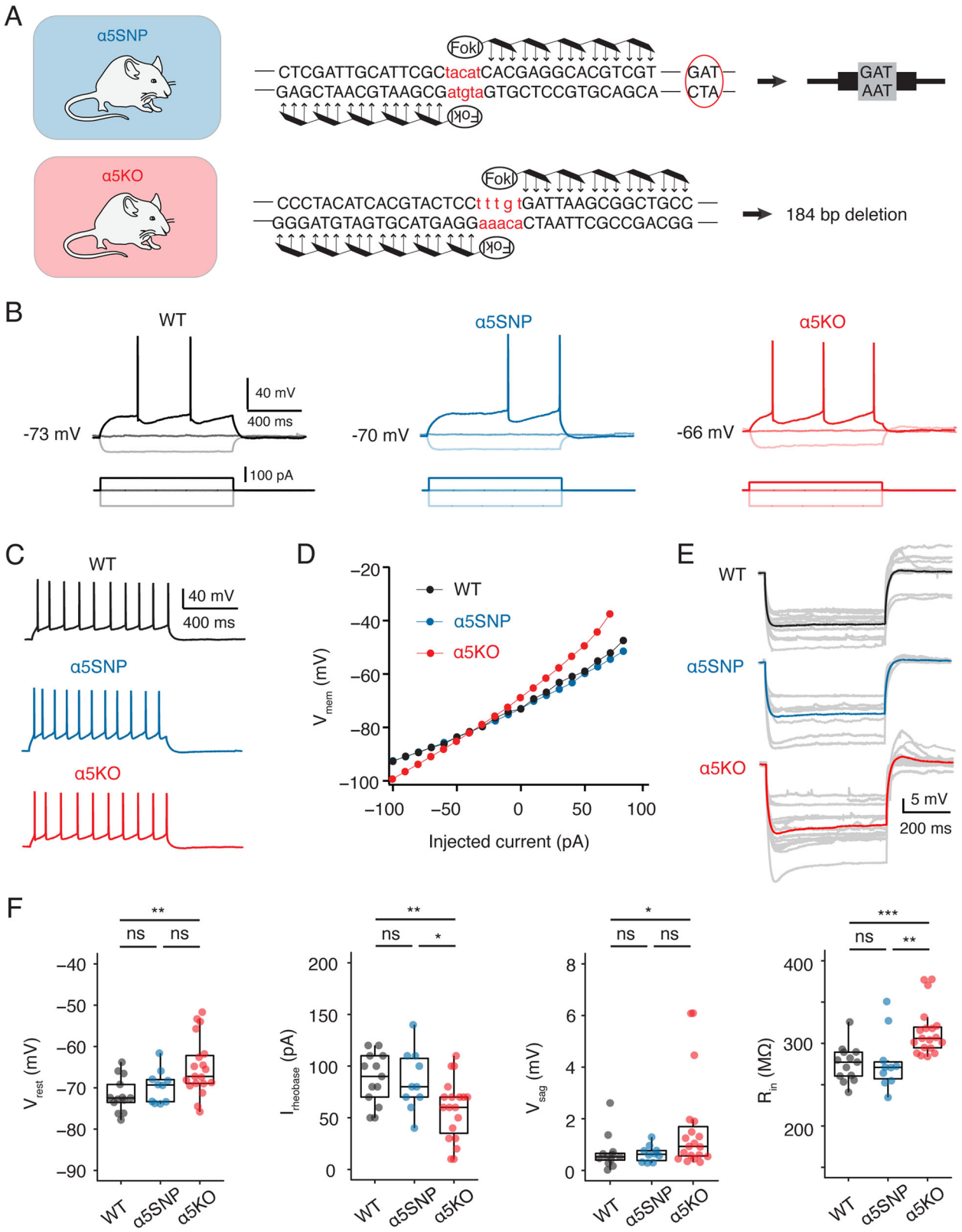

arborization of neurons in the α5KO group, L6 α5SNP neurons exhibited a greater total length of basal dendrites compared to neurons in the other two genotypes (Fig. 2C, Table S1). More details regarding morphological properties and statistical comparisons are given in Supplementary Table S1. Our findings suggest that morphological changes in L6 RS neuron dendrites, which depend on the α5 subunit, are evident in rats carrying the SNP and α5KO rats.

Fig. 1 L6 regular spiking (RS) neurons in α5KO rats show higher intrinsic excitability than those in WT and α5SNP rats. A Top, creation of α5SNP rats showing the insertion of the α5SNP at the end of the exon 5 of *Chrna5*. Bottom, creation of α5KO rats showing a 184-bp deletion in the gene *Chrna5*. **B** Representative AP firing of L6 RS neurons across three genotypes shows that L6 RS neurons in α5KO rats exhibit a more depolarized resting membrane potential and a smaller rheobase current compared to those in WT and α5 rats. AP firing (top) was elicited by a 1s square current of −100 pA, 0 pA, and rheobase current (bottom). **C** Representative firing patterns of the same L6 RS neurons shown in B. **D** I–V relationship of the same L6 RS neurons shown in B showing that the neuron in α5KO rat display a larger membrane input resistance than the other genotypes. **E** Voltage response to a hyperpolarizing step current of −100 pA and duration of 1s in L6 RS neurons from the three genotypes. Individual voltage traces are in gray and have been superimposed, average voltage traces for WT, α5SNP, and α5KO are shown in black, blue, and red, respectively. This illustrates that the L6 RS neuron in the α5KO rat shows a larger voltage sag compared to neurons in the other two genotypes. **F** Summary data of several electrophysiological properties of L6 RS neurons in WT, α5SNP, and α5KO rats showing that RS neurons in α5KO rats show higher intrinsic excitability than those in WT and α5SNP rats. Data were compared between WT (n = 13), α5SNP (n = 10), and α5KO (n = 19) groups and were presented as box plots,*P < 0.05, **P < 0.01, ***P < 0.001 for the Wilcoxon Mann–Whitney U test; ns, not significant.

Functional presence of α5 nAChR subunit correlates with dendritic spine density of L6 RS neurons

Previous studies revealed that dysfunction of high affinity nicotinic receptors or long term exposure of nicotinic agonist have an impact on dendritic spine density [56–59]. This phenomenon is also observed in L6 pyramidal cells of the mouse PFC lacking the α5 subunit in nicotinic receptors [41]. Here we analyzed the spine density in distal apical tuft as well as basal dendrite near the soma of L6 RS neurons in the three rat genotypes. Our results revealed that the complete deletion of the α5 nAChR subunit led to a substantial reduction in the spine density of apical tuft dendrites (0.21 ± 0.04 vs. 0.41 ± 0.10 μm^{-1}, ***P < 0.001). In contrast, neurons in the SNP group exhibited only a modest and statistically not significant decrease in the spine density of the apical dendrite (0.36 ± 0.09 vs. 0.41 ± 0.10 μm^{-1}, P = 0.514) (Fig. 3A). Furthermore, dysfunction of the α5 subunit also led to a gradual reduction in the basal dendritic spine density. In comparison to L6 excitatory neurons in WT rats, those in α5SNP and α5KO rats exhibited a significant decrease in basal dendritic spine density, namely 0.38 ± 0.09 μm^{-1} (*P < 0.05) and 0.30 ± 0.10 μm^{-1} (***P < 0.001), respectively, compared to 0.48 ± 0.07 μm^{-1} in WT rats (Fig. 3B).

To investigate whether the decrease in spine density resulted in a reduced spontaneous synaptic activity, we determined the frequency and amplitude of spontaneous excitatory postsynaptic potentials (sEPSPs) during continuous, 50 s long current-clamp recordings from L6 RS neurons (Fig. 3C, D). In parallel with a reduced functional expression of the α5 subunit, there was a gradual decrease in EPSP frequency. Neurons in the α5KO group showed a much lower EPSP frequency compared to WT neurons (1.40 ± 0.58 vs. 2.47 ± 0.54 Hz, ***P < 0.001) while α5SNP neurons displayed an intermediate value between the other two genotypes (Fig. 3E). Additionally, there was no discernible difference in the amplitude, decay time or rise time of spontaneous EPSPs among neurons in the WT, α5SNP, and α5KO groups (Fig. 3C, E). The data indicates that L6 RS neurons in mPFC of three rat genotypes differ significantly in spine density on their apical and basal dendrites, which is reflected in their spontaneous synaptic activity.

Galantamine acts as a positive allosteric modulator of α5*nAChRs in L6 RS neurons

To examine the nAChR responses in L6 of rat mPFC in isolation, we blocked muscarinic AChRs (mAChRs) by bath-applying 200 nM atropine in the perfusion ACSF and performed whole-cell recordings from L6 RS neurons. Following application of 10 μM acetylcholine (ACh) for 60 s, L6 RS neurons in WT rats showed an average membrane potential depolarization of 3.1 ± 3.2 mV. The vast majority of L6 RS neurons in α5SNP and α5KO rats showed weak to no depolarization following ACh application, as suggested by an average membrane potential change of 0.77 ± 0.73 mV and 0.93 ± 1.04 mV, respectively (Fig. 4A–C). Galantamine is a positive allosteric modulator (PAM) of α5*nAChRs at lower concentrations and also an inhibitor of acetylcholinesterase [17, 53]. To test whether galantamine exerts an allosteric modulation of nicotinic responses in L6 neurons, we pre-applied 1 μM galantamine for 10 min before and concurrently with ACh application. In the presence of galantamine, we observed a ~ 3.5-fold enhancement of the nicotinic ACh responses in the WT group, i.e., from 3.1 ± 3.2 to 11.7 ± 6.2 mV (***P < 0.001). In α5SNP rat neurons, galantamine significantly increased ACh-induced depolarization from 0.8 ± 0.7 to 5.5 ± 4.7 mV (***P < 0.001), leading to nicotinic responses comparable to the control level observed in WT neurons without the galantamine application (5.5 ± 4.7 vs. 3.1 ± 3.2 mV, P = 0.11) (Fig. 4B, C). This implies that galantamine functions as a PAM of α5*nAChRs and can restore the dysfunctional nAChR responses in L6 neurons of α5SNP rats to normal levels. In α5KO rat neurons, we found no statistically significant difference in ACh-induced responses before and after galantamine treatment (0.9 ± 1.0 vs. 1.2 ± 1.7 mV, P = 0.679), suggesting that galantamine specifically modulates α5*nAChRs (Fig. 4B, C).

Previous studies have demonstrated that α4β2*nAChRs locate specifically within mPFC L6 neurons [53, 60, 61], which is one of the known type of nAChRs that potentially includes α5 subunits as part of their assemblies [62]. The co-assembly of α5 subunits into α4β2*nAChRs enhances their Ca^{2+} permeability and slows down the receptor desensitization [16]. It has been shown that the deletion of the α5 subunit does not affect the density of α4β2 nAChRs but specifically reduces agonist activation affinity [55, 63]. Therefore we hypothesized that as a consequence of α5 subunit deletion, L6 neurons in the α5KO group require higher concentrations of ACh to activate nAChRs (Fig. 4D). To test this hypothesis, we puff-applied two high concentrations of ACh (100 μM and 1 mM) for 1 s sequentially on L6 RS neurons in WT and α5KO rats. Recordings were performed in the presence of 200 nM atropine and 0.5 μM tetrodotoxin (TTX) to block mAChRs and AP firing. Neurons in WT rats showed consistently strong depolarizations with a slight increase from 16.2 ± 7.3 to 19.8 ± 8.9 mV (*P < 0.05), in response to the puff-application of 100 μM and 1 mM ACh, respectively. In contrast, neurons in α5KO rats displayed a much greater depolarization following the application of 1 mM ACh compared to 100 μM ACh (14.7 ± 7.9 vs. 6.8 ± 4.9 mV ***P < 0.001) (Fig. 4E, F). A significant difference in the normalized amplitude of membrane potential change induced by 100 μM ACh (normalized to the effect of 1 mM ACh) was observed between L6 WT and α5KO neurons (Fig. 4G). In summary, dysfunction of the α5 nAChR subunit resulted in a shift of the ACh dose-response curve to higher concentrations, suggesting a potential mechanism underlying nicotine dependence.

Selective functional expression of the α5 nAChR subunit in L6 RS rather than BS neurons

In mPFC L6, a distinct population of excitatory neurons displaying burst-spiking (BS) firing patterns has been identified. While L6 corticothalamic neurons display a regular AP firing pattern, L6 corticocortical (CC) neurons tend to exhibit burst-spiking behavior [49, 50, 52, 64]. These neurons can be easily distinguished from RS

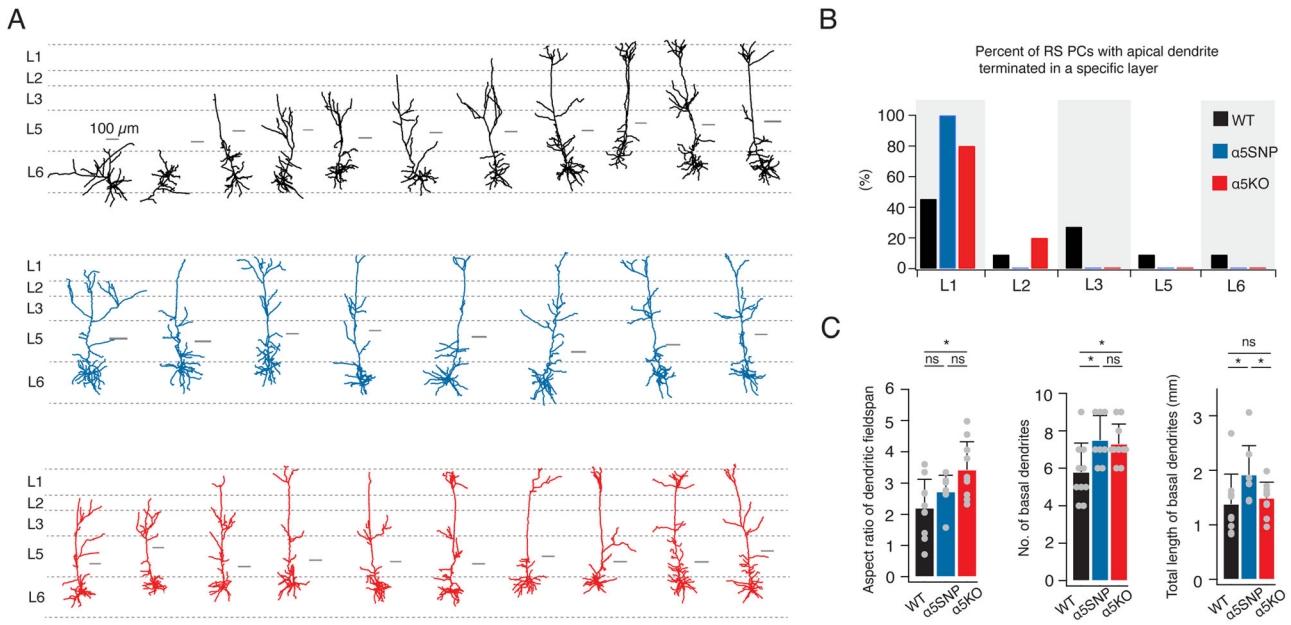

Fig. 2 Comparison of dendritic morphology of L6 RS neurons between WT, α5SNP, and KO genotypes. A Individual dendritic reconstruction of L6 RS neurons in the three rat genotypes. Neurons are shown in their laminar location with respect to averaged cortical layers, scale bar of each individual reconstruction is given. L6 RS neurons of WT (n = 11) rats are shown in black, α5SNP (n = 8) in blue, and α5KO (n = 10) in red. **B** Histograms of the percentage of L6 RS neurons with apical dendrite terminated in each cortical layer. L6 RS neurons of WT (n = 11) rats are shown in black, α5SNP (n = 8) in blue, and α5KO (n = 10) in red. Unlike RS neurons in WT rats, whose apical dendrites often terminate below L1, most neurons in α5SNP and α5KO rats have long apical dendrites extending into L1 of the mPFC. **C** Summary data of several morphological properties of L6 RS neurons in WT, α5SNP, and α5KO rats. Data were compared between WT (n = 11), α5SNP (n = 8), and α5KO (n = 10) groups, *P < 0.05 for the Wilcoxon Mann–Whitney U test; ns, not significant. Morphological changes in L6 RS neuron dendrites are evident for α5SNP and α5KO rats compared to WT rats.

neurons by their burst spiking pattern consisting of two or three initial, closely spaced APs (Fig. 5A). This is evident by a smaller second AP amplitude and a reduced adaptation ratio of the second versus tenth inter-spike intervals (ISI2/ISI10) compared to those of RS neurons (Fig. 5A, B). Notably, BS neurons display significantly weaker nicotinic responses compared to RS neurons in L6 of both rat barrel cortex and mPFC [53, 65]. To examine whether this is due to the absence of α5 subunit in BS neurons, we puff-applied 100 μM ACh for 1 s on L6 neurons in WT and α5KO rats. Recordings were conducted in the presence of 200 nM atropine and 0.5 μM tetrodotoxin (TTX) to exclude the influence of mAChR activation and AP firing. Consistent with previous findings, BS neurons showed a much smaller ACh-induced nicotinic response compared to RS neurons (4.4 ± 4.3 vs. 16.0 ± 7.5 mV, *P < 0.05) in WT rats (Fig. 5C, D). In α5KO rats, the deletion of the α5 nAChR subunit resulted in a decreased nicotinic response in RS neurons (6.1 ± 5.2 vs. 16.0 ± 7.5 mV, *P < 0.05). However, the amplitude of the ACh-induced depolarization in BS neurons remained unaffected compared to that in WT rats (2.3 ± 3.1 vs. 4.4 ± 4.3 mV, P = 0.352). This suggests that there is an absence of α5 subunit co-assembly in nAChRs on BS neurons, unlike RS neurons. It is worth noting that even in α5KO rats, BS neurons showed a smaller nicotinic response compared to RS neurons (2.3 ± 3.1 vs. 6.1 ± 5.2 mV, *P < 0.05) (Fig. 5D, E). This suggests a lower density of functional nAChR presence in L6 BS neurons, at least at the soma and the proximal dendrites.

We analyzed the electrophysiological properties of BS neurons in WT and α5KO rats. In Fig. 5F, ACh-induced membrane potential changes were plotted against the difference between the first and second AP amplitude, as well as the AP adaptation ratio. The 3D scatter plot revealed a strong correlation between cholinergic response and firing pattern-related properties for the two distinct types of excitatory neurons in L6. Moreover, the deletion of the α5 subunit in α5KO rats did not affect the electrophysiological properties of BS neurons, including resting membrane potential, rheobase current, voltage sag, and input resistance, which were not significantly different between WT and α5KO BS neurons (Fig. 5G). This lends further support to the idea that L6 BS excitatory neurons do not express the α5 nAChR subunit and hence only possess α4β2*nAChR.

Cell type-specific modulation of nAChRs by galantamine in human neocortical layer 6

For experiments on human L6 neurons, acute brain slices were prepared from tissue blocks obtained from brain surgery in six patients aged 23–66 years. The neocortical tissue used was from either the frontal, temporal or parietal cortex (Supplementary Table S2). It was resected during surgical access to the pathological brain region and was sufficiently distant from the pathological focus. Therefore, it can be considered as healthy cortex (Fig. 6A). Whole-cell current clamp recordings with simultaneous biocytin filling were made from human cortical L6 neurons allowing post-hoc identification of their morphology. To analyze the repetitive AP firing properties of L6 neurons, voltage recordings were used in which a current injection elicited ~10 APs. Similar to observations in rodents, two distinct firing patterns were identified in human L6 excitatory neurons: regular or burst spiking (Fig. 6B). In contrast to human L6 RS neurons, which exhibited nearly constant AP amplitudes throughout the train, BS neurons often displayed a spike burst at the onset of the AP train, with a smaller second AP amplitude and subsequent recovery in AP magnitude (Fig. 6C). Moreover, RS neurons exhibited either a single AP or a spike doublet that occurred at the beginning of the AP train and was followed by APs with nearly constant ISIs. In contrast, BS neurons displayed an initial long ISI but a shorter stable ISIs thereafter following the initial AP burst (Fig. 6C). Notably, at the rheobase current injection, a spike doublet was only observed for BS but not RS neurons (Fig. 6B). Significant

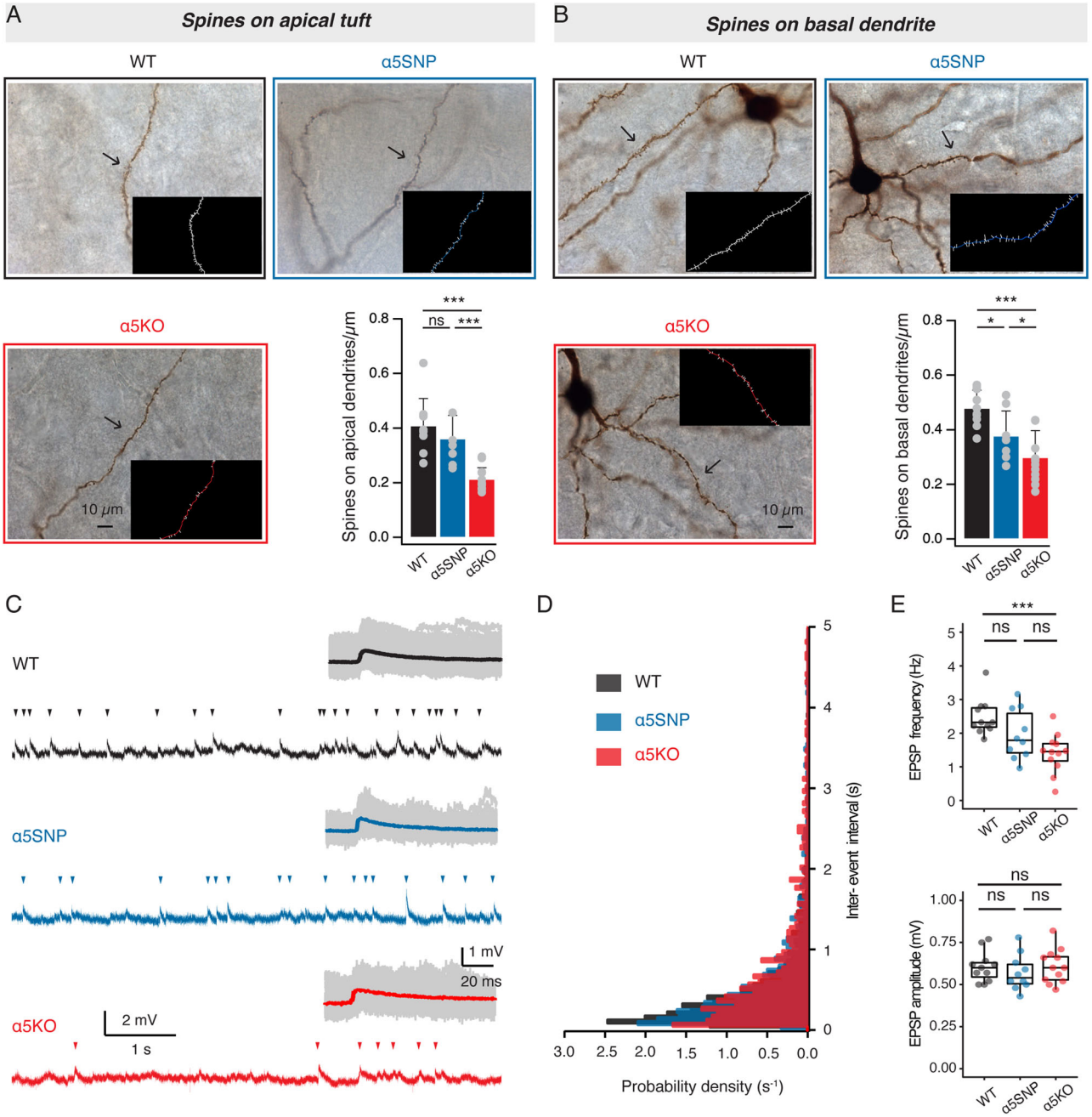

Fig. 3 Down-regulation or depletion of α5 subunit confers a decrease of dendritic spine density and EPSP frequency in L6 RS neurons. **A** Photomicrographs of biocytin-filled apical tuft of a representative L6 RS neuron in a WT, α5SNP, and α5KO rat. Insets showing counted dendritic spines of marked branch. Spine density on the apical tuft was modestly decreased in neurons from α5SNP rats (n = 7) but substantially decreased in neurons from α5KO rats (n = 10) compared to neurons from WT rats (n = 8), ***P < 0.001 for the Wilcoxon Mann–Whitney U test; ns, not significant. **B** Photomicrographs of biocytin-filled basal dendrites of a representative L6 RS neuron in a WT, α5SNP, and α5KO rat. Insets showing counted dendritic spines of marked branch. Compared to neurons in WT rats (n = 8), spine density on basal dendrites was significantly decreased in neurons from α5SNP (n = 7) and α5KO (n = 10) rats, *P < 0.05, ***P < 0.001 for the Wilcoxon Mann–Whitney U test. **C** A 7 s V_m recording of L6 RS neurons across three genotypes shows a gradual decrease in EPSP frequency in WT, α5SNP, and α5KO rats. Excitatory postsynaptic potentials (EPSPs) are marked by arrowheads. Insets displaying the overlay of EPSPs extracted from a 20 s continuous recording of the same neurons. The average and individual EPSPs are superimposed and given in a color and gray shade, respectively. **D** Histograms showing probability density of inter-event interval (IEI) between two consecutive EPSPs indicate a gradual increase in EPSP IEI in WT, α5SNP, and α5KO rats. Data were collected and analyzed from 50 s continuous recordings of 11 L6 RS neurons in WT rats (n = 1299 events), 10 neurons in α5SNP rats (n = 828 events), and 12 neurons in α5KO rats (n = 622 events). **E** Box plots comparing EPSP frequency and amplitude of L6 RS neurons in WT (n = 11 neurons), α5SNP (n = 10 neurons), and α5KO rats (n = 12 neurons); *** P < 0.001 for the Wilcoxon Mann–Whitney U test; ns, not significant.

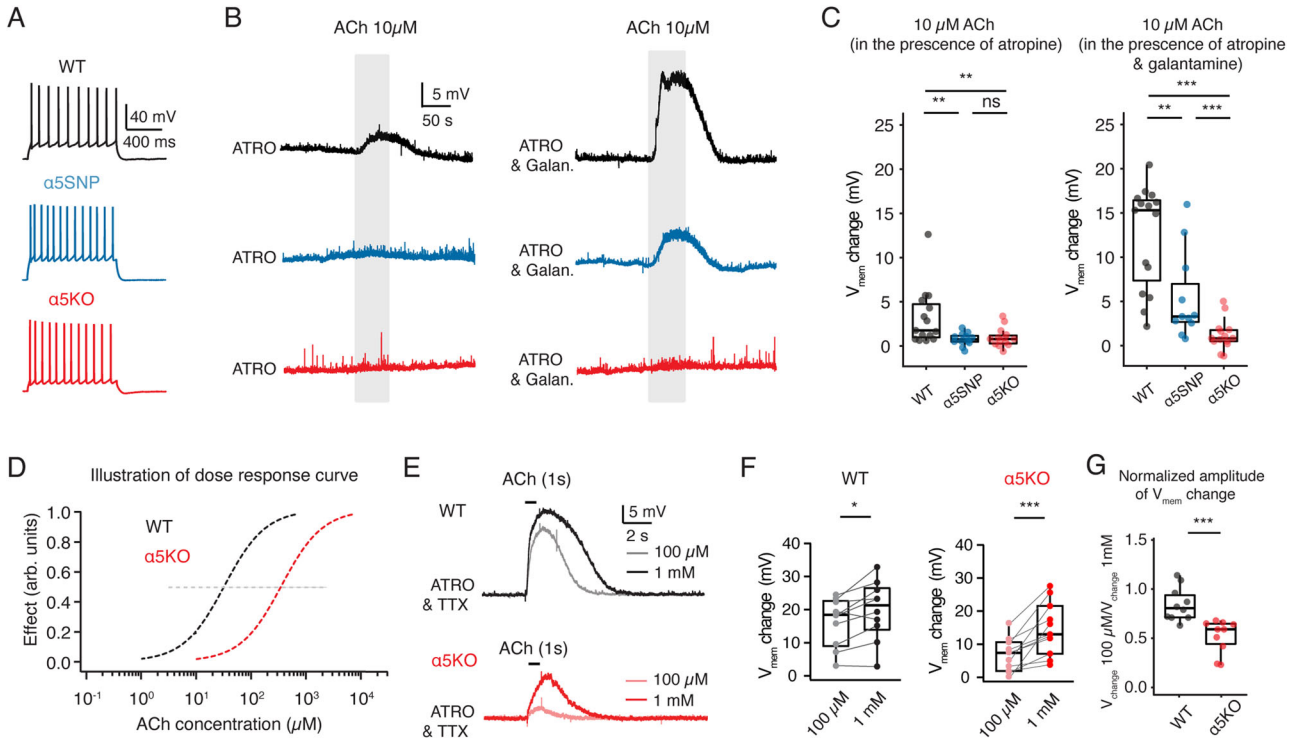

Fig. 4 Galantamine acts as a positive allosteric modulator of α5*nAChRs in L6 RS neurons. A Representative firing patterns of a L6 RS neuron recorded in WT α5SNP and α5KO rat, respectively. **B** Bath application of a low concentration of ACh (10 μM, 50 s) to L6 RS neurons was enhanced in the presence of 1 μM galantamine in WT and α5SNP rats, but not in α5KO rats, compared to the absence of galantamine. Recordings were performed in the presence of 200 nM atropine to rule out the muscarinic receptor activation. Representative recording traces are shown in balck for WT neuron, blue for α5SNP neuron, and red for α5KO neuron, respectively. **C** Summary box plots showing the ACh (10 μM) induced resting membrane potential (Vm) change under control and galantamine (1 μM) conditions in L6 RS neurons in WT (n = 16 neurons), α5SNP (n = 12 neurons) and α5KO rats (n = 15 neurons). While ACh depolarized L6 RS neurons in WT rats, it induced weak to no depolarization in L6 RS neurons of α5SNP and α5KO rats. Pre-application of 1 μM galantamine increased ACh-induced depolarization in L6 RS neurons of WT and α5SNP rats, resulting in distinct V_m changes among the three groups. **P < 0.01, ***P < 0.001 for the Wilcoxon Mann–Whitney U test; ns, not significant. **D** As a consequence of deletion of α5 subunits,ACh activate nAChRs of L6 RS neurons in WT rats at significantly lower concentrations than in α5KO rats, as can be seen from the illustration of dose–response curves; the grey dashed line marks the EC50 for the curves. **E** Representative traces of puff-applied ACh at 100 μM and 1 mM concentrations for 1 s in L6 RS neuron in a WT (top, black) and α5KO (bottom, red) rat. Recordings were performed in the presence of 200 nM atropine and 0.5 μM tetrodotoxin (TTX) to block mAChRs activation and AP firing. ACh-evoked Vm depolarization is smaller in KO rat but shows a substantial increase when using high concentration of 1 mM ACh when compared to 100 μM. **F** Box plots show that ACh-evoked (1 s puff-applied) depolarizations of L6 RS neurons increased as ACh concentrations were raised from 100 μM to 1 mM in both WT (n = 10 neurons) and α5KO (n = 11 neurons) rats. *P < 0.05, ***P < 0.001 for Wilcoxon signed-rank test. **G** Normalized amplitude of Vmem change (Vmem change 100 μM/Vmem change 1 mM) showing that a significant difference in dose-dependent responses between L6 RS neurons in WT (n = 10 neurons) and α5KO (n = 11 neurons) rats.

differences in the adaptation ratio, voltage sag and frequency-current slope were found between human RS and BS excitatory neurons (Fig. 6C and Supplementary Table S3). More electrophysiological properties and the statistical comparison of the two neuron types are given in Supplementary Table S3.

To examine the nicotinic responses in L6 of human neocortex, we blocked mAChRs by bath-applying 200 nM atropine in the perfusion ACSF. Following bath-application of 10 μM ACh, both human L6 RS and BS neurons showed a membrane potential depolarization of 3.0 ± 2.8 mV and 3.1 ± 3.1 mV, respectively. To identify whether the ACh response can be potentiated, 1 μM galantamine was pre-applied for 10 min before the ACh application. The majority of the RS neurons showed a significant increase in the nicotinic response from 3.0 ± 2.8 to 8.6 ± 4.9 mV (**P < 0.01) following the galantamine treatment, indicating the presence of α5*nAChRs. In contrast, the ACh response in L6 BS neurons was not changed by galantamine (3.1 ± 3.1 vs. 2.9 ± 2.3 mV, P = 0.884) (Fig. 6D, E).

To compare the morphological differences between two types of L6 neurons, we performed 3D reconstructions of the somato-dendritic domain of RS and BS neurons in the human neocortex. RS neurons exclusively have an upright projecting apical dendrite that terminates within the range of cortical L1 to L5 while, BS neurons display various morphologies including small pyramidal cells, multipolar, or bipolar neurons (Fig. 6F). On average, RS neurons showed a larger vertical dendritic fieldspan (1.6 ± 0.3 vs. 1.2 ± 0.4 mm, *P < 0.05), resulting in a greater aspect ratio of dendritic fieldspan when compared to BS neurons (2.9 ± 0.6 vs. 1.5 ± 0.5, ***P < 0.001). Furthermore, a significant proportion of BS neurons exhibited a multipolar morphology (5 out of 9), so that on average, BS neurons showed a greater length of the longest basal dendrite compared to RS neurons (4.0 ± 2.6 vs. 1.6 ± 0.8 mm, *P < 0.05) (Fig. 6G). Additional morphological properties and statistical comparisons of the two neuron types are presented in Supplementary Table S3.

DISCUSSION

In this study, we conducted whole-cell patch clamp recordings from L6 RS neurons in the mPFC of WT, α5SNP, and α5KO rats. We found that the deletion of the α5 subunit significantly altered the intrinsic membrane properties, spine density, and dendritic morphology of L6 RS neurons. On the other hand, the presence of an α5SNP mutation affected spine distribution and dendritic

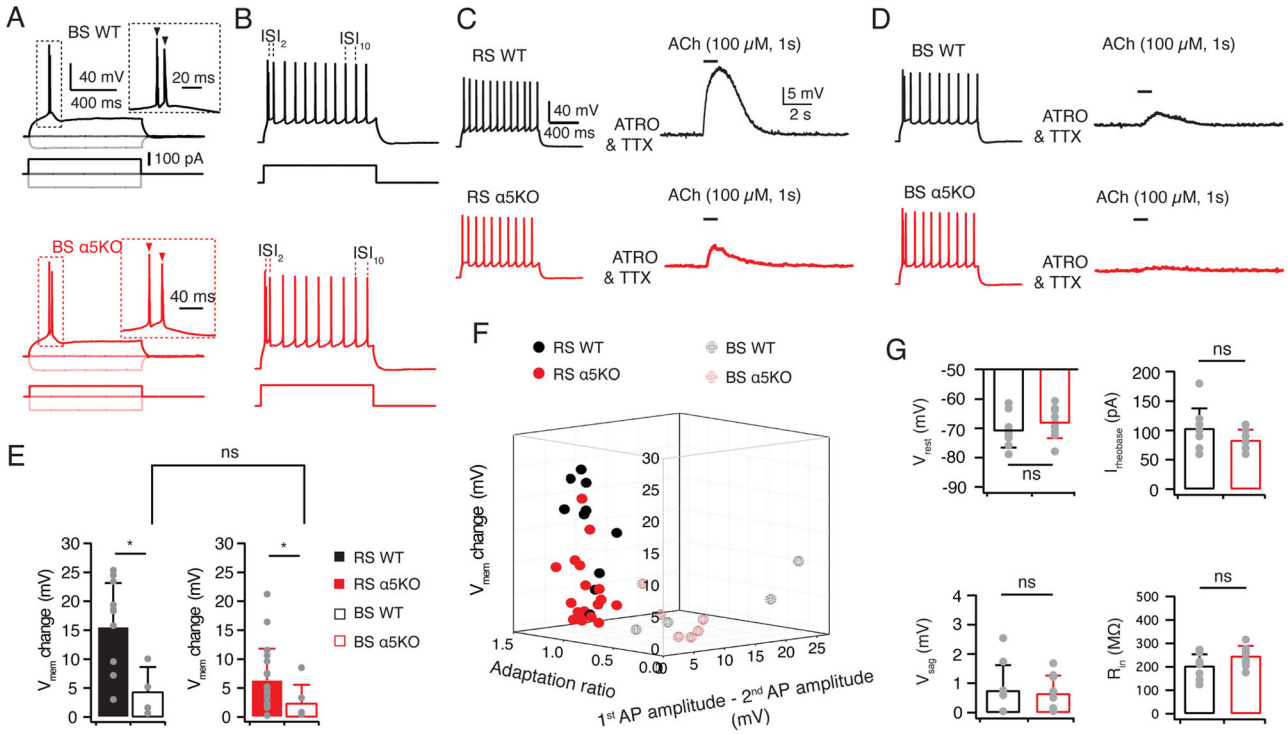

Fig. 5 α5 subunits are abundantly expressed in L6 RS neurons but not in busrt spiking (BS) neurons. A Representative AP firing of a L6 BS neuron in a WT, α5SNP, and α5KO rat. AP-firing (top) was elicited in response to 1 s square current of −100 pA, 0 pA, and rheobase current (bottom). Insets showing initial AP bursts at an expanded time scale. **B** Corresponding firing patterns of representative BS neurons shown in A. Injected current pulses are shown at the bottom. **C** Representative traces of puff-applied 100 μM ACh for 1 s in a L6 RS neuron in a WT (top, black) and α5KO (bottom, red) rat. Recordings were performed in the presence of 200 nM atropine and 0.5 μM tetrodotoxin (TTX) to block mAChR activation and AP firing. ACh-evoked depolarizations are smaller in α5KO compared to WT rat. The corresponding firing patterns of the neurons are shown on the left. **D** Representative traces of puff-applied 100 μM ACh for 1 s in a L6 BS neuron in a WT (top, black) and α5KO (bottom, red) rat. Recordings were performed in the presence of 200 nM atropine and 0.5 μM tetrodotoxin (TTX) to block mAChR activation and AP firing. The ACh-evoked depolarization is small both in WT and α5KO rat. The corresponding firing patterns are shown on the left. **E** Summary histograms showing that puff application of ACh (100 μM) induces smaller depolarization in L6 BS neurons than RS neurons in both WT (n = 14 for RS neurons and n = 4 for BS neurons) and α5KO rats (n = 23 for RS neurons and n = 5 for BS neurons). *P < 0.05 for the Wilcoxon Mann–Whitney U test; ns, not significant. **F** 3D scatter plot indicate a clear separation of L6 RS and BC neuron subtypes based on their electrophysiological properties and ACh-induced Vmem changes. Neurons recorded from WT rats are shown in black and those from α5KO rats in red. **G** Histograms of electrophysiological properties of L6 BS neurons show no significant differences between WT (n = 9, black) and α5KO (n = 9, red) rats. Statistical analysis was performed using the Wilcoxon Mann–Whitney U test; ns, not significant.

arborizations without altering intrinsic electrophysiological properties. Furthermore, our findings revealed the crucial role of the α5 subunit encoded by *Chrna5* in generating nicotinic responses in response to low concentrations of ACh. Galantamine, a PAM of α5*nAChRs, effectively restored the ACh-induced nicotinic modulation in neurons of α5SNP rats to levels observed in WT rats but had no effect in neurons of α5KO rats. Additionally, we found that the functional distribution of the α5 subunit is cell-type specific, with a notably more prominent presence in RS neurons compared to BS neurons. This observation was consistent in both rat and human neocortical L6.

Aberrant neuronal properties due to the loss or partial loss of function in the α5 subunit

Previous studies showed no significant differences in passive properties, including input resistance and resting membrane potential, between neurons in WT and α5KO mice. This observation applies to neurons located in both the mouse rostral interpeduncular nucleus and RS neurons in L6 of the mouse mPFC, which are two sites characterized by remarkably high *Chrna5* mRNA expression levels in rodents [61, 66]. In marked contrast, we observed that α5 deletion in the created KO rat line caused significant alterations in several electrophysiological characteristics of L6 RS neurons, including the resting membrane potential, input resistance, rheobase current, and voltage sag. This may be due to species differences between transgenic mice and rats. We then analyzed the same properties of L6 RS neurons in mPFC of rats carrying the human α5SNP rs16969968. This genetic variant is highly prevalent in the general population, with a frequency of 37% in Europeans and 50% in Middle Eastern populations. It has been proven to be a risk factor for nicotine dependence and SZ [29, 33, 67]. In vitro data suggests that the α5SNP results in a partial loss of function in nAChRs when co-assembled with α4β2* subunits, potentially forming either (α4β2)2α5 or α4(β2)2α6α5 combinations [19, 68–70]. However, genotype-dependent differences in the electrophysiological properties were not observed between WT and α5SNP rats.

It has been demonstrated that the functional expression of the α5 subunit mediates a developmental retraction of apical dendrites in L6 neurons. Neurons in WT mice, but not α5KO mice, exhibit a notable shift towards shorter apical dendrites by early adulthood [55]. Here, we conducted a comparative analysis of the dendritic morphology of L6 RS neurons among the three genotypes using young adult rats. Our findings indicate that the expression of the rs16969968 SNP induces changes in morphological features resembling those observed in α5KO rats, with the majority of neurons having a long apical dendrite that extending into superficial layers. In addition to its effects on dendritic morphology, nicotine exposure or nAChR dysfunction also has powerful effects on dendritic spine density [41, 56–59]. Consistent

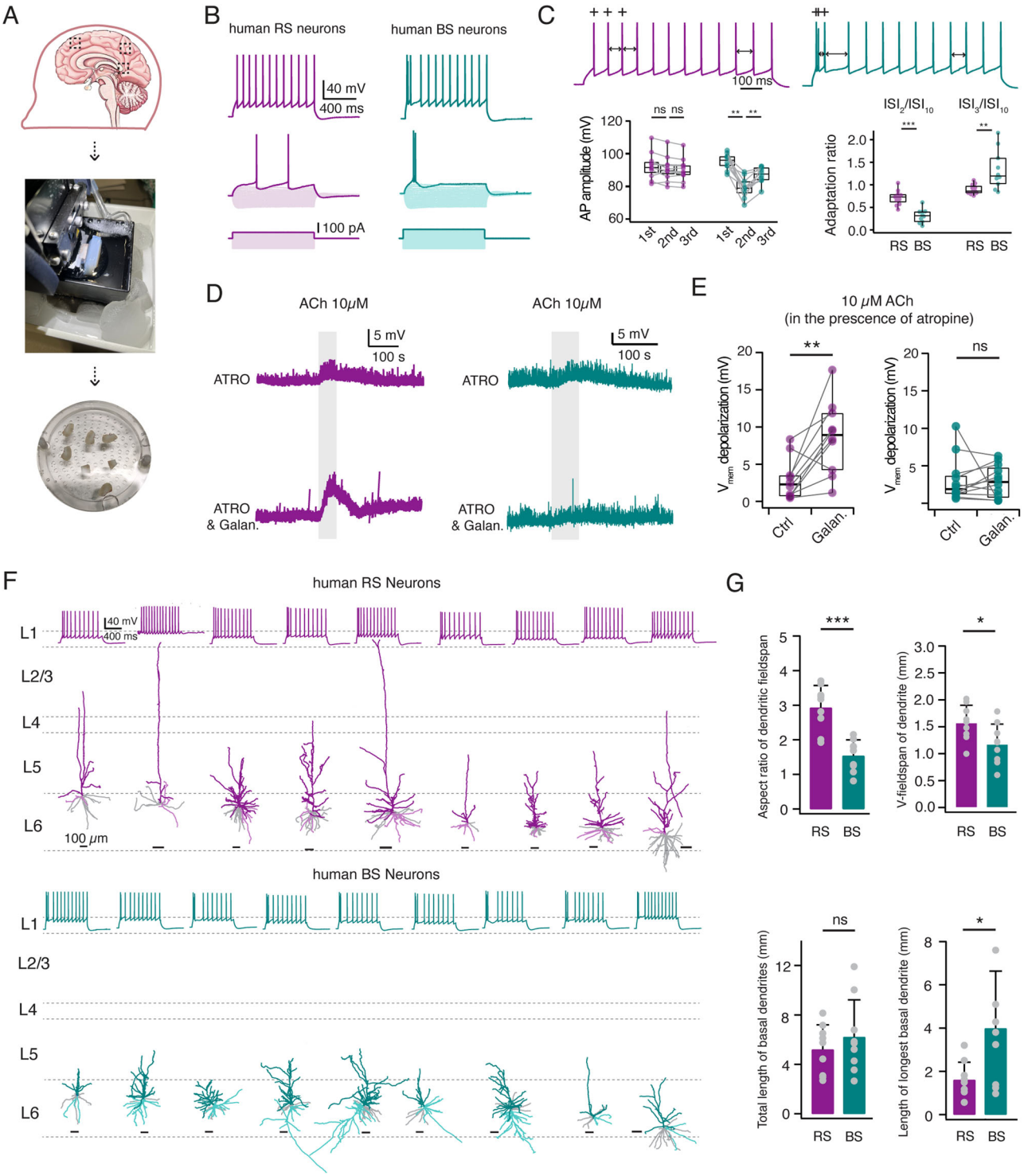

with this idea, we observed a gradual decrease in dendritic spine density among L6 RS neurons in WT, α5SNP-carrying, and α5KO rats. The aberrant dendritic morphology and altered spine density of L6 RS neurons in mPFC of α5SNP rats serve as structural correlates of abnormal synaptic plasticity and cortical output resulting from α5 nAChR subunit dysfunction. These changes could potentially contribute to the pathophysiology of neuropsychiatric disorders such as attention-deficit disorder and SZ, which result from the impairment of PFC function [71, 72].

Potential therapeutic strategies to address cognitive deficits by targeting the α5 nicotinic subunit

It has been shown that in humans the presence of α5SNP rs16969968 decreases resting state functional connectivity of a dorsal anterior cingulate-ventral striatum/extended amygdala circuit. The activity of this circuits predicts addiction severity in smokers and is further impaired in people with mental illnesses [35]. Similarly, in the PFC of α5SNP rs16969968-expressing mice, lower activity of vasoactive intestinal polypeptide (VIP) interneurons resulted in an increased somatostatin (SOM) interneuron

Fig. 6 Glantamine acts as a positive allosteric modulator of nAChRs in human L6 RS but not BS neurons. A Summary procedure of acute human brain slice preparation. **B** Top, representative firing patterns of a human L6 RS (left) and BS neuron (right). Bottom, AP-firing was elicited in response to 1 s square current using a step size increment of 10 pA from −100 pA to its rheobase current. **C** Top, Representative firing patterns at an expanded time scale show a clear distinction in AP firing pattern between human L6 RS and BS neurons. The first three APs are marked by +. The second, third, and tenth inter-spike interval are marked by bidirectional arrows. Bottom left, box plots comparing the first, second, and third AP amplitude of human L6 RS (n = 11) and BS (n = 11) neurons. RS neurons exhibited constant AP amplitudes, while BS neurons showed a smaller second AP amplitude followed by recovery in the third. **P < 0.01 for Wilcoxon signed-rank test; ns, not significant. Bottom right, box plots comparing spiking adaptation between RS and BS neurons. BS neurons exhibited a shorter ISI_2/ISI_{10} and a longer ISI_3/ISI_{10} in comparison to RS neurons. **P < 0.01, ***P < 0.001 for Wilcoxon Mann–Whitney U test. **D** In the presence of 1 μM galantamine, bath application of a low concentration ACh (10 μM, 50 s) induces a larger depolarization in human L6 RS but not in BS neurons compared to the absence of galantamine. Recordings were performed in the presence of 200 nM atropine to block mAChR activation. Representative recordings are shown in purple for RS neurons while in teal for BS neurons. **E** Box plots showing that galantamine enhances ACh-induced depolarization of human L6 RS neurons (n = 10) but not BS neurons (n = 11). **P < 0.01 for Wilcoxon signed-rank test; ns, not significant. **F** Dendritic reconstructions of individual human L6 RS and BS neurons show that RS neurons have an exclusively upright projecting apical dendrite. In contrast, BS neurons display a heterogeneous dendritic morphology. Neurons are shown in their laminar location with respect to averaged cortical layers, scale bar of each individual reconstruction is given. Apical dendrites of RS neurons (n = 9) are shown in purple and BS neurons (n = 9) in teal. The longest basal dendrite of neurons are given in lighter shade, the other basal dendrites in gray. Top traces shows the corresponding firing pattern of each neuron. **G** Histograms comparing several dendritic properties between L6 RS (n = 9) and BS (n = 9) neurons. *P < 0.05, **P < 0.01 for Wilcoxon signed-rank test; ns, not significant.

inhibitory drive over L2/3 pyramidal neurons. The decreased activity observed in α5SNP-expressing mice can be reversed by chronic nicotine administration [36]. These studies provide a physiological basis for the tendency of SZ patients carrying α5SNP to self-medicate by smoking. Given the prevalence of the rs16969968 in the general human population, homozygous carriers may benefit from medication that could potentially restore a partial loss of function of the corresponding nAChR subtype. This may help address nicotine addiction and cognitive impairment among patients with SZ. Therefore, it is of great interest to develop pharmacological interventions to ameliorate the relevant dysfunction. Small molecules, such as galantamine, can act as PAMs of channel function in the high-affinity α5*nAChRs. At low concentrations, galantamine binds allosterically to nAChRs and enhances their function; at high concentrations, it also acts as a weak acetylcholinesterase (AChE) inhibitor [17, 53]. Here, we used transgenic rats to compare different genotypes with respect to their nicotinic responses and modulation by galantamine. Following application of 10 μM ACh, only L6 RS neurons in WT rats showed a membrane potential depolarization while neurons in α5SNP and α5KO rats displayed no response. This suggests an essential role of α5*nAChRs in tonic cholinergic neuromodulation mediated by volume transmission [8, 73]. Notably, the application of 1 μM galantamine successfully restored nicotinic responses in L6 neurons of α5SNP rats to WT level. This potentiation effect, however, was not observed in α5KO rats. Our results indicate that galantamine or its derivatives could be a potential pharmacological therapy with high specificity for improving the function of high-affinity nAChRs in populations carrying the rs16969968 polymorphism.

As an AChE inhibitor, galantamine has long been used to treat the cognitive impairments in Alzheimer's disease [74, 75]. There is growing evidence that galantamine can improve cognitive function in psychiatric disorders including SZ [76–78], major depression [79–81], bipolar disorder [82, 83], and alcohol dependence [84]. These therapeutic effects may result from the allosterically potentiating role of galantamine, which contributes not only to increased nAChR signaling but also to the enhancement of the release of other neurotransmitters such as glutamate, dopamine and noradrenaline [85–87]. The administration of galantamine has been shown to attenuate nicotine intake and seeking behavior in rats [88]. This effect is relevant in the context of the rs16969968 polymorphism, which is associated with a relapse to nicotine seeking in transgenic rats carrying this α5SNP [37]. Using the same α5SNP rats, we demonstrated that galantamine can ameliorate abnormal nAChR responses in the PFC L6 neuronal circuitry. The behavioral consequences of galantamine administration in the α5SNP rats remain to be fully elucidated. Further research is required to investigate the impact of galantamine on the reduced resting-state functional connectivity and alterations in neuronal circuits involving the PFC in rats with this SNP, as well as its potential for recovering the related cognitive and behavioral deficits [36, 37].

Functional distribution of the α5 subunit is cell type-specific

Two main pyramidal cell populations exist in neocortical layer 6: RS CT neurons and BS CC neurons [49, 50, 52, 64]. By forming reciprocal interactions between the PFC and thalamic nuclei, CT cells are an essential part of the cortico-thalamo-cortical feedback loop, which plays a critical role in cognition [89, 90]. On the other hand, CC neurons send long-range efferents that can innervate other subregions of the PFC, contralateral PFC, and other intratelencephalic targets [91, 92]. Due to the severe truncation of axons in brain slices, it is generally not possible to fully recover the axonal morphologies of pyramidal neurons in human neocortex. Although this limitation is significant, as the axonal morphology distinguishes CT from CC neurons, previous studies have reliably linked RS and BS firing patterns to the morphology of CT and CC cells, respectively [49, 52]. Thus, our functional classification of CT and CC neurons based on firing patterns remains valid.

It has been shown that nicotinic currents in L6 neocortical BS neurons are weaker compared to RS neurons [53, 65]. Here, we provide strong evidence for a selective functional expression of *Chrna5* in L6 of rat mPFC. The small nAChR-mediated depolarization in BS neurons can be attributed to both a low density of α4ß2* nAChRs and the absence of co-assembly with the α5 subunit. Deletion of the α5 subunit resulted in a reduced nicotinic response in RS neurons but not BS neurons. This suggests the absence of α4ß2α5 nAChRs in BS neurons. This finding is consistent with a study that used in situ hybridization to demonstrate selective expression of *Chrna5* in CT neurons in mouse primary somatosensory cortex [54]. In α5KO rats, we also observed a weaker nAChR-mediated depolarization in BS neurons compared to RS neurons, indicating a lower density of nAChRs composed solely of α4 and ß2 nAChR subunits.

Recent studies have combined single cell-electrophysiology, morphology, and transcriptomics to perform a more comprehensive cell type classification of human cortical neurons [93–96]. However, there is still a lack of studies exploring the combination of transcriptomic and morpho-electric properties in human cortical layer 6, which remains a missing domain. Using human cortical samples obtained during brain surgery, we identified a cell type-specific expression of α5*nAChRs in human neocortical layer

6. The nAChR-mediated effects were found to be closely related to both neuronal firing pattern and dendritic morphology. In contrast to L6 RS neurons, which uniformly display upright-oriented apical dendrites, BS neurons exhibit a more heterogeneous morphology including small pyramids, multipolar neurons, and bipolar neurons, consistent with previous studies for CC neurons [97, 98]. Due to the scarcity of human brain samples, our study did not exclusively target the frontal lobe but encompassed additional regions including the temporal and parietal cortices. These brain regions exhibit functional overlap and uniformly express the *CHRNA5* gene [99, 100]. Since the rat data exclusively pertain to the mPFC, greater caution is required when try to extrapolate these findings to human data.

CONCLUSION

In summary, we have shown that L6 RS CT neurons are more efficiently modulated by ACh than BS CC neurons due to the presence of α5*nAChR. As an integral part of the cortico-thalamo-cortical pathway, L6 CT neurons in PFC provide feedback control of thalamo-frontal circuitry, contributing to the maintenance of persistent activity in the higher-order thalamus during behavior [90]. Dysfunctions in the thalamic counterparts of PFC, or thalamo-frontal circuitry have been implicated in various neuropsychiatric disorders including SZ [38, 39, 101]. Our findings improve our understanding of cholinergic modulation of neuronal microcircuits involved in cognition and highlight a potential pharmacological target for restoring nicotinic signaling under pathological conditions. The potential of galantamine and its derivatives may represent a promising avenue for pharmacological interventions to improve nAChR functionality, particularly in individuals carrying the rs16969968 polymorphism. This has significant implications for the treatment of cognitive impairments and nicotine addiction, particularly in patients with SZ. Understanding the cell type-specific expression of α5*nAChRs can inform the development of new treatments that more effectively target specific neuronal populations, potentially minimizing side effects. These insights underscore the broader clinical relevance of this study and suggest potential applications for targeted therapies in neuropsychiatric conditions.

DATA AVAILABILITY

The datasets generated and analyzed during the current study are available from the corresponding author on reasonable request.

CODE AVAILABILITY

All the custom-written code used in the study is available from the corresponding author on reasonable request.

REFERENCES

1. Hasselmo ME. The role of acetylcholine in learning and memory. Curr Opin Neurobiol. 2006;16:710–5.
2. Herrero JL, Roberts MJ, Delicato LS, Gieselmann MA, Dayan P, Thiele A. Acetylcholine contributes through muscarinic receptors to attentional modulation in V1. Nature. 2008;454:1110–4.
3. Hasselmo ME, Sarter M. Modes and models of forebrain cholinergic neuromodulation of cognition. Neuropsychopharmacology. 2011;36:52–73.
4. Eggermann E, Kremer Y, Crochet S, Petersen CCH. Cholinergic signals in mouse barrel cortex during active whisker sensing. Cell Rep. 2014;9:1654–60.
5. Ma S, Hangya B, Leonard CS, Wisden W, Gundlach AL. Dual-transmitter systems regulating arousal, attention, learning and memory. Neurosci Biobehav Rev. 2018;85:21–33.
6. Goldman-Rakic PS. Cellular basis of working memory. Neuron. 1995;14:477–85.
7. Passetti F, Dalley JW, O'Connell MT, Everitt BJ, Robbins TW. Increased acetylcholine release in the rat medial prefrontal cortex during performance of a visual attentional task. Eur J Neurosci. 2000;12:3051–8.
8. Parikh V, Kozak R, Martinez V, Sarter M. Prefrontal acetylcholine release controls cue detection on multiple timescales. Neuron. 2007;56:141–54.
9. Gritton HJ, Howe WM, Mallory CS, Hetrick VL, Berke JD, Sarter M. Cortical cholinergic signaling controls the detection of cues. Proc Natl Acad Sci USA. 2016;113:E1089–1097.
10. Howe WM, Gritton HJ, Lusk NA, Roberts EA, Hetrick VL, Berke JD, et al. Acetylcholine release in prefrontal cortex promotes gamma oscillations and theta-gamma coupling during cue detection. J Neurosci. 2017;37:3215–30.
11. Perry DC, Xiao Y, Nguyen HN, Musachio JL, Davila-Garcia MI, Kellar KJ. Measuring nicotinic receptors with characteristics of alpha4beta2, alpha3beta2 and alpha3beta4 subtypes in rat tissues by autoradiography. J Neurochem. 2002;82:468–81.
12. Gotti C, Zoli M, Clementi F. Brain nicotinic acetylcholine receptors: native subtypes and their relevance. Trends Pharmacol Sci. 2006;27:482–91.
13. Gotti C, Clementi F, Fornari A, Gaimarri A, Guiducci S, Manfredi I, et al. Structural and functional diversity of native brain neuronal nicotinic receptors. Biochem Pharmacol. 2009;78:703–11.
14. Wada E, McKinnon D, Heinemann S, Patrick J, Swanson LW. The distribution of mRNA encoded by a new member of the neuronal nicotinic acetylcholine receptor gene family (alpha 5) in the rat central nervous system. Brain Res. 1990;526:45–53.
15. Winzer-Serhan UH, Leslie FM. Expression of alpha5 nicotinic acetylcholine receptor subunit mRNA during hippocampal and cortical development. J Comp Neurol. 2005;481:19–30.
16. Fucile S. Ca2+ permeability of nicotinic acetylcholine receptors. Cell Calcium. 2004;35:1–8.
17. Kuryatov A, Onksen J, Lindstrom J. Roles of accessory subunits in alpha4beta2(*) nicotinic receptors. Mol Pharmacol. 2008;74:132–43.
18. Bailey CD, De Biasi M, Fletcher PJ, Lambe EK. The nicotinic acetylcholine receptor alpha5 subunit plays a key role in attention circuitry and accuracy. J Neurosci. 2010;30:9241–52.
19. Maskos U. The nicotinic receptor alpha5 coding polymorphism rs16969968 as a major target in disease: functional dissection and remaining challenges. J Neurochem. 2020;154:241–50.
20. Hung RJ, McKay JD, Gaborieau V, Boffetta P, Hashibe M, Zaridze D, et al. A susceptibility locus for lung cancer maps to nicotinic acetylcholine receptor subunit genes on 15q25. Nature. 2008;452:633–7.
21. Tobacco and Genetics Consortium. Genome-wide meta-analyses identify multiple loci associated with smoking behavior. Nat Genet. 2010;42:441–7.
22. Taylor AE, Morris RW, Fluharty ME, Bjorngaard JH, Asvold BO, Gabrielsen ME, et al. Stratification by smoking status reveals an association of CHRNA5-A3-B4 genotype with body mass index in never smokers. PLoS Genet. 2014;10:e1004799.
23. Sakornsakolpat P, Prokopenko D, Lamontagne M, Reeve NF, Guyatt AL, Jackson VE, et al. Genetic landscape of chronic obstructive pulmonary disease identifies heterogeneous cell-type and phenotype associations. Nat Genet. 2019;51:494–505.
24. Grucza RA, Wang JC, Stitzel JA, Hinrichs AL, Saccone SF, Saccone NL, et al. A risk allele for nicotine dependence in CHRNA5 is a protective allele for cocaine dependence. Biol Psychiatry. 2008;64:922–9.
25. Wang JC, Grucza R, Cruchaga C, Hinrichs AL, Bertelsen S, Budde JP, et al. Genetic variation in the CHRNA5 gene affects mRNA levels and is associated with risk for alcohol dependence. Mol Psychiatry. 2009;14:501–10.
26. Sherva R, Kranzler HR, Yu Y, Logue MW, Poling J, Arias AJ, et al. Variation in nicotinic acetylcholine receptor genes is associated with multiple substance dependence phenotypes. Neuropsychopharmacology. 2010;35:1921–31.
27. Lubke GH, Stephens SH, Lessem JM, Hewitt JK, Ehringer MA. The CHRNA5/A3/B4 gene cluster and tobacco, alcohol, cannabis, inhalants and other substance use initiation: replication and new findings using mixture analyses. Behav Genet. 2012;42:636–46.
28. Schizophrenia Working Group of the Psychiatric Genomics C. Biological insights from 108 schizophrenia-associated genetic loci. Nature. 2014;511:421–7.
29. Bierut LJ, Stitzel JA, Wang JC, Hinrichs AL, Grucza RA, Xuei X, et al. Variants in nicotinic receptors and risk for nicotine dependence. Am J Psychiatry. 2008;165:1163–71.
30. Wang JC, Cruchaga C, Saccone NL, Bertelsen S, Liu P, Budde JP, et al. Risk for nicotine dependence and lung cancer is conferred by mRNA expression levels and amino acid change in CHRNA5. Hum Mol Genet. 2009;18:3125–35.
31. Pandey N, Pal S, Sharma LK, Guleria R, Mohan A, Srivastava T. SNP rs16969968 as a strong predictor of nicotine dependence and lung cancer risk in a North Indian population. Asian Pac J Cancer Prev. 2017;18:3073–9.
32. Thorgeirsson TE, Geller F, Sulem P, Rafnar T, Wiste A, Magnusson KP, et al. A variant associated with nicotine dependence, lung cancer and peripheral arterial disease. Nature. 2008;452:638–42.

33. Saccone NL, Wang JC, Breslau N, Johnson EO, Hatsukami D, Saccone SF, et al. The CHRNA5-CHRNA3-CHRNB4 nicotinic receptor subunit gene cluster affects risk for nicotine dependence in African-Americans and in European-Americans. Cancer Res. 2009;69:6848–56.
34. Ware JJ, van den Bree MB, Munafo MR. Association of the CHRNA5-A3-B4 gene cluster with heaviness of smoking: a meta-analysis. Nicotine Tob Res. 2011;13:1167–75.
35. Hong LE, Hodgkinson CA, Yang Y, Sampath H, Ross TJ, Buchholz B, et al. A genetically modulated, intrinsic cingulate circuit supports human nicotine addiction. Proc Natl Acad Sci USA. 2010;107:13509–14.
36. Koukouli F, Rooy M, Tziotis D, Sailor KA, O'Neill HC, Levenga J, et al. Nicotine reverses hypofrontality in animal models of addiction and schizophrenia. Nat Med. 2017;23:347–54.
37. Forget B, Scholze P, Langa F, Morel C, Pons S, Mondoloni S, et al. A human polymorphism in CHRNA5 is linked to relapse to nicotine seeking in transgenic rats. Curr Biol. 2018;28:3244–53.e3247
38. Giraldo-Chica M, Woodward ND. Review of thalamocortical resting-state fMRI studies in schizophrenia. Schizophr Res. 2017;180:58–63.
39. Parnaudeau S, Bolkan SS, Kellendonk C. The mediodorsal thalamus: an essential partner of the prefrontal cortex for cognition. Biol Psychiatry. 2018;83:648–56.
40. Proulx E, Piva M, Tian MK, Bailey CD, Lambe EK. Nicotinic acetylcholine receptors in attention circuitry: the role of layer VI neurons of prefrontal cortex. Cell Mol Life Sci. 2014;71:1225–44.
41. Kang L, Tian MK, Bailey CD, Lambe EK. Dendritic spine density of prefrontal layer 6 pyramidal neurons in relation to apical dendrite sculpting by nicotinic acetylcholine receptors. Front Cell Neurosci. 2015;9:398.
42. Gabbott PL, Warner TA, Jays PR, Salway P, Busby SJ. Prefrontal cortex in the rat: projections to subcortical autonomic, motor, and limbic centers. J Comp Neurol. 2005;492:145–77.
43. van Aerde KI, Feldmeyer D. Morphological and physiological characterization of pyramidal neuron subtypes in rat medial prefrontal cortex. Cereb Cortex. 2015;25:788–805.
44. Mitric M, Seewald A, Moschetti G, Sacerdote P, Ferraguti F, Kummer KK, et al. Layer-and subregion-specific electrophysiological and morphological changes of the medial prefrontal cortex in a mouse model of neuropathic pain. Sci Rep. 2019;9:9479.
45. Ding C, Emmenegger V, Schaffrath K, Feldmeyer D. Layer-specific inhibitory microcircuits of layer 6 interneurons in rat prefrontal cortex. Cereb Cortex. 2021;31:32–47.
46. Schwarz N, Uysal B, Welzer M, Bahr JC, Layer N, Loffler H, et al. Long-term adult human brain slice cultures as a model system to study human CNS circuitry and disease. Elife. 2019;8:e48417.
47. Marx M, Gunter RH, Hucko W, Radnikow G, Feldmeyer D. Improved biocytin labeling and neuronal 3D reconstruction. Nat Protoc. 2012;7:394–407.
48. Noether GE. Sample-size determination for some common nonparametric-tests. J Am Stat Assoc. 1987;82:645–7.
49. Kumar P, Ohana O. Inter- and intralaminar subcircuits of excitatory and inhibitory neurons in layer 6a of the rat barrel cortex. J Neurophysiol. 2008;100:1909–22.
50. Tian MK, Bailey CD, Lambe EK. Cholinergic excitation in mouse primary vs. associative cortex: region-specific magnitude and receptor balance. Eur J Neurosci. 2014;40:2608–18.
51. Cotel F, Fletcher LN, Kalita-de Croft S, Apergis-Schoute J, Williams SR. Cell class-dependent intracortical connectivity and output dynamics of layer 6 projection neurons of the rat primary visual cortex. Cereb Cortex. 2018;28:2340–50.
52. Yang D, Qi G, Ding C, Feldmeyer D. Layer 6A pyramidal cell subtypes form synaptic microcircuits with distinct functional and structural properties. Cereb Cortex. 2022;32:2095–111.
53. Kassam SM, Herman PM, Goodfellow NM, Alves NC, Lambe EK. Developmental excitation of corticothalamic neurons by nicotinic acetylcholine receptors. J Neurosci. 2008;28:8756–64.
54. Sorensen SA, Bernard A, Menon V, Royall JJ, Glattfelder KJ, Desta T, et al. Correlated gene expression and target specificity demonstrate excitatory projection neuron diversity. Cereb Cortex. 2015;25:433–49.
55. Bailey CD, Alves NC, Nashmi R, De Biasi M, Lambe EK. Nicotinic alpha5 subunits drive developmental changes in the activation and morphology of prefrontal cortex layer VI neurons. Biol Psychiatry. 2012;71:120–8.
56. Brown RW, Kolb B. Nicotine sensitization increases dendritic length and spine density in the nucleus accumbens and cingulate cortex. Brain Res. 2001;899:94–100.
57. Ballesteros-Yanez I, Benavides-Piccione R, Bourgeois JP, Changeux JP, DeFelipe J. Alterations of cortical pyramidal neurons in mice lacking high-affinity nicotinic receptors. Proc Natl Acad Sci USA. 2010;107:11567–72.
58. Lozada AF, Wang X, Gounko NV, Massey KA, Duan J, Liu Z, et al. Induction of dendritic spines by beta2-containing nicotinic receptors. J Neurosci. 2012;32:8391–400.
59. Mychasiuk R, Muhammad A, Gibb R, Kolb B. Long-term alterations to dendritic morphology and spine density associated with prenatal exposure to nicotine. Brain Res. 2013;1499:53–60.
60. Guillem K, Bloem B, Poorthuis RB, Loos M, Smit AB, Maskos U, et al. Nicotinic acetylcholine receptor beta2 subunits in the medial prefrontal cortex control attention. Science. 2011;333:888–91.
61. Morton G, Nasirova N, Sparks DW, Brodsky M, Sivakumaran S, Lambe EK, et al. Chrna5-expressing neurons in the interpeduncular nucleus mediate aversion primed by prior stimulation or nicotine exposure. J Neurosci. 2018;38:6900–20.
62. Hay YA, Lambolez B, Tricoire L. Nicotinic transmission onto layer 6 cortical neurons relies on synaptic activation of Non-alpha7 receptors. Cereb Cortex. 2016;26:2549–62.
63. Brown RW, Collins AC, Lindstrom JM, Whiteaker P. Nicotinic alpha5 subunit deletion locally reduces high-affinity agonist activation without altering nicotinic receptor numbers. J Neurochem. 2007;103:204–15.
64. Mercer A, West DC, Morris OT, Kirchhecker S, Kerkhoff JE, Thomson AM. Excitatory connections made by presynaptic cortico-cortical pyramidal cells in layer 6 of the neocortex. Cereb Cortex. 2005;15:1485–96.
65. Yang D, Gunter R, Qi G, Radnikow G, Feldmeyer D. Muscarinic and nicotinic modulation of neocortical layer 6A synaptic microcircuits is cooperative and cell-specific. Cereb Cortex. 2020;30:3528–42.
66. Venkatesan S, Lambe EK. Chrna5 is essential for a rapid and protected response to optogenetic release of endogenous acetylcholine in prefrontal cortex. J Neurosci. 2020;40:7255–68.
67. Hong LE, Yang X, Wonodi I, Hodgkinson CA, Goldman D, Stine OC, et al. A CHRNA5 allele related to nicotine addiction and schizophrenia. Genes Brain Behav. 2011;10:530–5.
68. Kuryatov A, Berrettini W, Lindstrom J. Acetylcholine receptor (AChR) alpha5 subunit variant associated with risk for nicotine dependence and lung cancer reduces (alpha4beta2)(2)alpha5 AChR function. Mol Pharmacol. 2011;79:119–25.
69. Sciaccaluga M, Moriconi C, Martinello K, Catalano M, Bermudez I, Stitzel JA, et al. Crucial role of nicotinic alpha5 subunit variants for Ca2+ fluxes in ventral midbrain neurons. FASEB J. 2015;29:3389–98.
70. Deflorio C, Blanchard S, Carisi MC, Bohl D, Maskos U. Human polymorphisms in nicotinic receptors: a functional analysis in iPS-derived dopaminergic neurons. FASEB J. 2017;31:828–39.
71. Barch DM, Carter CS, Braver TS, Sabb FW, MacDonald A 3rd, Noll DC, et al. Selective deficits in prefrontal cortex function in medication-naive patients with schizophrenia. Arch Gen Psychiatry. 2001;58:280–8.
72. Dalley JW, Theobald DE, Bouger P, Chudasama Y, Cardinal RN, Robbins TW. Cortical cholinergic function and deficits in visual attentional performance in rats following 192 IgG-saporin-induced lesions of the medial prefrontal cortex. Cereb Cortex. 2004;14:922–32.
73. Sarter M, Parikh V, Howe WM. Phasic acetylcholine release and the volume transmission hypothesis: time to move on. Nat Rev Neurosci. 2009;10:383–90.
74. Olin J, Schneider L. Galantamine for Alzheimer's disease. Cochrane Database Syst Rev. 2002;3:CD001747.
75. Loy C, Schneider L. Galantamine for Alzheimer's disease and mild cognitive impairment. Cochrane Database Syst Rev. 2006;2006:CD001747.
76. Allen TB, McEvoy JP. Galantamine for treatment-resistant schizophrenia. Am J Psychiatry. 2002;159:1244–5.
77. Schubert MH, Young KA, Hicks PB. Galantamine improves cognition in schizophrenic patients stabilized on risperidone. Biol Psychiatry. 2006;60:530–3.
78. Buchanan RW, Conley RR, Dickinson D, Ball MP, Feldman S, Gold JM, et al. Galantamine for the treatment of cognitive impairments in people with schizophrenia. Am J Psychiatry. 2008;165:82–9.
79. Elgamal S, MacQueen G. Galantamine as an adjunctive treatment in major depression. J Clin Psychopharmacol. 2008;28:357–9.
80. Holtzheimer PE 3rd, Meeks TW, Kelley ME, Mufti M, Young R, McWhorter K, et al. A double blind, placebo-controlled pilot study of galantamine augmentation of antidepressant treatment in older adults with major depression. Int J Geriatr Psychiatry. 2008;23:625–31.
81. Biard K, Douglass AB, De Koninck J. The effects of galantamine and buspirone on sleep structure: implications for understanding sleep abnormalities in major depression. J Psychopharmacol. 2015;29:1106–11.
82. Schrauwen E, Ghaemi SN. Galantamine treatment of cognitive impairment in bipolar disorder: four cases. Bipolar Disord. 2006;8:196–9.

83. Ghaemi SN, Gilmer WS, Dunn RT, Hanlon RE, Kemp DE, Bauer AD, et al. A double-blind, placebo-controlled pilot study of galantamine to improve cognitive dysfunction in minimally symptomatic bipolar disorder. J Clin Psychopharmacol. 2009;29:291–5.
84. Mann K, Ackermann K, Diehl A, Ebert D, Mundle G, Nakovics H, et al. Galantamine: a cholinergic patch in the treatment of alcoholism: a randomized, placebo-controlled trial. Psychopharmacology. 2006;184:115–21.
85. Sharp BM, Yatsula M, Fu Y. Effects of galantamine, a nicotinic allosteric potentiating ligand, on nicotine-induced catecholamine release in hippocampus and nucleus accumbens of rats. J Pharmacol Exp Ther. 2004;309:1116–23.
86. Konradsson-Geuken A, Wu HQ, Gash CR, Alexander KS, Campbell A, Sozeri Y, et al. Cortical kynurenic acid bi-directionally modulates prefrontal glutamate levels as assessed by microdialysis and rapid electrochemistry. Neuroscience. 2010;169:1848–59.
87. Noda Y, Mouri A, Ando Y, Waki Y, Yamada SN, Yoshimi A, et al. Galantamine ameliorates the impairment of recognition memory in mice repeatedly treated with methamphetamine: involvement of allosteric potentiation of nicotinic acetylcholine receptors and dopaminergic-ERK1/2 systems. Int J Neuropsychopharmacol. 2010;13:1343–54.
88. Hopkins TJ, Rupprecht LE, Hayes MR, Blendy JA, Schmidt HD. Galantamine, an acetylcholinesterase inhibitor and positive allosteric modulator of nicotinic acetylcholine receptors, attenuates nicotine taking and seeking in rats. Neuropsychopharmacology. 2012;37:2310–21.
89. Parnaudeau S, O'Neill PK, Bolkan SS, Ward RD, Abbas AI, Roth BL, et al. Inhibition of mediodorsal thalamus disrupts thalamofrontal connectivity and cognition. Neuron. 2013;77:1151–62.
90. Collins DP, Anastasiades PG, Marlin JJ, Carter AG. Reciprocal circuits linking the prefrontal cortex with dorsal and ventral thalamic nuclei. Neuron. 2018;98:366–79.e364
91. Briggs F. Organizing principles of cortical layer 6. Front Neural Circuits. 2010;4:3.
92. Harris KD, Shepherd GM. The neocortical circuit: themes and variations. Nat Neurosci. 2015;18:170–81.
93. Berg J, Sorensen SA, Ting JT, Miller JA, Chartrand T, Buchin A, et al. Human neocortical expansion involves glutamatergic neuron diversification. Nature. 2021;598:151–8.
94. Kalmbach BE, Hodge RD, Jorstad NL, Owen S, de Frates R, Yanny AM, et al. Signature morpho-electric, transcriptomic, and dendritic properties of human layer 5 neocortical pyramidal neurons. Neuron. 2021;109:2914–27.e2915
95. Chartrand T, Dalley R, Close J, Goriounova NA, Lee BR, Mann R, et al. Morpho-electric and transcriptomic divergence of the layer 1 interneuron repertoire in human versus mouse neocortex. Science. 2023;382:eadf0805.
96. Lee BR, Dalley R, Miller JA, Chartrand T, Close J, Mann R, et al. Signature morphoelectric properties of diverse GABAergic interneurons in the human neocortex. Science. 2023;382:eadf6484.
97. Zhang ZW, Deschenes M. Intracortical axonal projections of lamina VI cells of the primary somatosensory cortex in the rat: a single-cell labeling study. J Neurosci. 1997;17:6365–79.
98. Thomson AM. Neocortical layer 6, a review. Front Neuroanat. 2010;4:13.
99. Hawrylycz MJ, Lein ES, Guillozet-Bongaarts AL, Shen EH, Ng L, Miller JA, et al. An anatomically comprehensive atlas of the adult human brain transcriptome. Nature. 2012;489:391–9.
100. Allen Human Brain Atlas. https://human.brain-map.org/, 2014.
101. Bradfield LA, Hart G, Balleine BW. The role of the anterior, mediodorsal, and parafascicular thalamus in instrumental conditioning. Front Syst Neurosci. 2013;7:51.

ACKNOWLEDGEMENTS

We would like to thank Werner Hucko for excellent technical assistance. We thank Dr. Karlijn van Aerde for custom-written macros in Igor Pro software. We thank Yutong Wu for reconstructing 3D dendritic morphologies of both rat and human neurons and Dr. Henner Koch and Aniella Bak for kind help with human slice preparations. We are grateful for funding from the European Union's Horizon 2020 Framework Programme for Research and Innovation under the Framework Partnership Agreement No. 650003 (HBP FPA) to D.F.

AUTHOR CONTRIBUTIONS

DF, DY, and GQ designed the experiments. DY and GQ carried out the patch-clamp recording experiments from human and rat slices and performed electrophysiological data analysis. DY performed morphological and spine analysis. DD performed surgeries on human patients. UM provided the transgenetic rat models. DY and DF wrote the manuscript with the inputs from all authors. All authors have given approval for the final version of the manuscript.

FUNDING

Open Access funding enabled and organized by Projekt DEAL.

COMPETING INTERESTS

The authors declare no competing interests.

ETHICS APPROVAL

All experimental procedures involving animals were performed in accordance with the guidelines of the Federation of European Laboratory Animal Science Associations (FELASA), the EU Directive 2010/63/EU, and the German Animal Welfare Law. For research involving human tissues, the study was reviewed and approved by the ethics committee of RWTH Aachen University Hospital (EK067/20).

INFORMED CONSENT

Written informed consent was obtained from all patients for the use of spare neocortical tissue acquired during surgical procedures.

ADDITIONAL INFORMATION

Supplementary information The online version contains supplementary material available at https://doi.org/10.1038/s41398-025-03230-9.

Correspondence and requests for materials should be addressed to Danqing Yang or Dirk Feldmeyer.

Reprints and permission information is available at http://www.nature.com/reprints

Publisher's note Springer Nature remains neutral with regard to jurisdictional claims in published maps and institutional affiliations.